Tissue Eng Regen Med (2022) 19(5):1001–1012
https://doi.org/10.1007/s13770-022-00480-2

Online ISSN 2212-5469

ORIGINAL ARTICLE

# Graded-Three-Dimensional Cell-Encapsulating Hydrogel as a Potential Biologic Scaffold for Disc Tissue Engineering

**Zhixiang Li[1,2] · Yiwen Zhang[1,3] · Yupeng Zhao[1] · Xubin Gao[1] · Zhonglian Zhu[1] · Yingji Mao[1,2] · Taibao Qian[1,2]**

Received: 24 May 2022 / Revised: 30 June 2022 / Accepted: 3 July 2022 / Published online: 13 August 2022


## Abstract

***BACKGROUND:*** Intervertebral disk (IVD) degeneration, which can cause lower back pain, is a major predisposing factor for disability and can be managed through multiple approaches. However, there is no satisfactory strategy currently available to reconstruct and recover the natural properties of IVDs after degeneration. As tissue engineering develops, scaffolds with embedded cell cultures have proved critical for the successful regeneration of IVDs.

***METHODS:*** In this study, an integrated scaffold for IVD replacement was developed. Through scanning electron microscopy and other mechanical measurements, we characterized the physical properties of different hydrogels. In addition, we simulated the physiological structure of natural IVDs. Nucleus pulposus (NP) cells and annulus fibrosus-derived stem cells (AFSCs) were seeded in gelatin methacrylate (GelMA) hydrogel at different concentrations to evaluate cell viability and matrix expression.

***RESULTS:*** It was found that different concentrations of GelMA hydrogel can provide a suitable environment for cell survival. However, hydrogels with different mechanical properties influence cell adhesion and extracellular matrix component type I collagen, type II collagen, and aggrecan expression.

***CONCLUSION:*** This tissue-engineered IVD implant had a similar structure and function as the native IVD, with the inner area mimicking the NP tissue and the outer area mimicking the stratified annulus fibrosus tissue. The new integrated scaffold demonstrated a good simulation of disc structure. The preparation of efficient and regeneration-promoting tissue-engineered scaffolds is an important issue that needs to be explored in the future. It is hoped that this work will provide new ideas and methods for the further construction of functional tissue replacement discs.

**Keywords** Hydrogel · Gelatin methacrylate · Intervertebral disk replacement

Zhixiang Li, Yiwen Zhang and Yupeng Zhao have been contributed equally to this work.

✉ Yingji Mao
maoyingji252@yeah.net

✉ Taibao Qian
taibaoqian@126.com

[1] Department of Orthopedics, First Affiliated Hospital, School of Life Sciences, Bengbu Medical College, Bengbu 233030, China

[2] Anhui Province Key Laboratory of Tissue Transplantation, Bengbu Medical College, Bengbu 233030, China

[3] Department of Plastic Surgery and Burn Center, Second Affiliated Hospital, Plastic Surgery Institute of Shantou University Medical College, Shantou 515063, Guangdong, China

## 1 Introduction

Intervertebral disk (IVD) degeneration is a common cause of lower back pain. Globally, approximately 84% of people have a lifetime prevalence of IVD disorders; among these, approximately 10% will succumb to IVD degeneration and thereby develop chronic disability. The high disability resulting from IVD degeneration considerably increases the burden of medical costs on society [1–3]. However, therapies against IVD degeneration are currently limited. Conservative treatment and surgery are common approaches. Conservative treatment includes traction, massage, physiotherapy, and non-steroidal drug use, whereas surgery includes removing herniated nucleus pulposus (NP), bone grafting, and metal implants. Unfortunately, both strategies can only alleviate symptoms, such as reducing pain or recovering partial intrinsic properties of the IVD. Additionally, the height- and weight-bearing capabilities of the IVD are difficult to restore despite good surgical outcomes. Moreover, there is a high risk of IVD degeneration due to a decrease in the stability of the body's biomechanics. Internal fixation with large metal implants may also cause unknown complications. In this context, new effective therapeutic strategies are urgently needed to combat IVD diseases [4–7].

In normal cases, human IVDs are located between the superior and inferior vertebral bodies—a closed microenvironment comprising the NP, annulus fibrosus (AF), and superior and inferior cartilage endplates [8, 9]. In the process of IVD degeneration, NP tissue changes are an early indicator, such as decreased cell count, protein expression, and inflammation processes [10]. The dehydrated state of the NP causes an uneven stress dispersion of the axial load on the adjacent vertebrae, further leading to the destruction of the surrounding elastic fibers [11]. Most importantly, the altered microenvironment makes it challenging for nutrient-deficient cells to complete endogenous repair [12]. To achieve effective and precise disc repair, we use tissue engineering techniques, such as cell therapy. Since NP cells (NPCs) play an important role in maintaining IVD homeostasis, NPC transplantation can compensate for the loss of cells in degenerative disc disease, making it an effective strategy for treating disc degeneration. Annulus fibrosus-derived stem cells (AFSCs) have multi-differentiation potential. While possessing high biological activity, they can specifically differentiate into AF cells under the regulation of certain targeted factors. Thus, cell therapy offers a potential treatment for degenerative disc disease. The NP tissue belongs to an immune-specific zone that can allow the proliferation, differentiation, and expression of the extracellular matrix surrounding the transplanted cells [13, 14]. However, in the case of disc degeneration, the altered microenvironment is not sufficient to support the viable state of the transplanted cells. Therefore, we need to apply a scaffold that can act as a carrier, promoting cell survival and maintaining the physiological activity of the cells while also being able to mimic the physical properties of the IVD by acting as a bionic scaffold.

Tissue engineering techniques have created the conditions for the development of regenerative medicine [15–17]. These techniques are an important aspect of regenerative medicine that combines cell transplantation and scaffolds to promote tissue regeneration. In recent years, an increasing number of biological materials have been used in tissue regeneration. Hydrogels are considered promising biomaterials for bionic tissue engineering based on a similar structure to that of natural tissue [18]. Hydrogels have gained attention due to their high water content and good mechanical properties. Currently, the hydrogels used to evaluate disc bionic scaffolds include sodium alginate [19], chitosan [20], collagen [21], and fibrin [22]. Bionic collagen microchannel scaffolds implanted in spinal cord injuries have shown a significant effect on nerve regeneration while allowing cell survival [23]. Photopolymerized bioadhesive hydrogels have shown outstanding advantages in regenerative medicine, for example in wound repair [24], bone defect treatment [25], and corneal transplantation [26, 27]. However, hydrogel-mimicking disc bionic scaffolds in IVDs are rarely available. Optimally, a three-dimensional microenvironmentally functional bionic material that mimics the physiological structure of a natural IVD requires certain biological properties, such as degradability, good biocompatibility, and the ability to promote cell proliferation and secretion of exosomes. More importantly, since the function is impaired in IVD degeneration, biomaterials need appropriate mechanical properties. However, most of the developed hydrogels do not meet the above requirements. For example, collagen is not widely used owing to its poor mechanical properties and degradability, and fibrin gel is not stable.

Gelatin methacrylate (GelMA) is a photosensitive hydrogel that is capable of liquid-to-solid conversion through initiator cross-linking and UV light. Most importantly, we can control the mechanical properties and degradability of the hydrogel by adjusting the GelMA ratio or the time of photo-crosslinking [28], allowing precise control of the mechanical properties of the bionic disc scaffold. Some studies have found that 5% GelMA hydrogels can better promote NPC survival, proliferation, and protein expression owing to good biocompatibility[11]. For spinal cord injury repair, 5% GelMA hydrogels have a significant facilitative effect [29]. Moreover, GelMA hydrogels have been applied in cartilage regeneration

[30–32], nerve regeneration [29, 33], osteogenesis [34, 35], tumor treatment [36, 37] and wound healing [38]. Most importantly, in addition to the high water content, the porous structure is a crucial feature of the GelMA hydrogel [39], imitating the properties of natural IVD tissue, facilitating the transport of nutrients, and providing a suitable environment for the transplanted cells. For these reasons, we considered GelMA hydrogel a promising candidate for a bionic IVD scaffold.

In this study, we investigated the physical properties of the hydrogel by adjusting the GelMA hydrogel concentration and performing transplantation of AFSCs and NPCs, while also evaluating the bioactivity of the cells in the hydrogel scaffold. Subsequently, a bionic disc scaffold was constructed using hydrogels with different mechanical properties to encapsulate the cells, presenting a novel idea for disc regeneration.

## 2 Materials and methods

### 2.1 Preparation and characterization of the GelMA hydrogels

#### *2.1.1 Sample fabrication*

The synthesis of GelMA has been described in the literature [40]. In brief, methacrylate anhydride (EFL, Suzhou, China) was gradually dissolved in the gelatin solution, consisting of gelatin (EFL) and pre-warmed phosphate buffer solution (PBS; Gibco, Shanghai, China). After a 2-h reaction, the mixture was dialyzed through dialysis bags (MW: 8000–14 000) to eliminate unbound impurities. After seven consecutive days of dialysis, the dialysate was heated to 60 °C and filtered using a 0.22-μm membrane filter (Biosharp, Hefei, China). The filtrate was then freeze-dried and the obtained white solid was prepared for subsequent experiments.

For the fabrication of the 5% (w/v) GelMA hydrogel, 5 g of GelMA were added into the 100 mL standard solution of 0.25% (w/v) photo-initiator (EFL) dissolved in PBS (0.01 M, pH 7.4). Followed by sterilization with a 0.22 μm sterile needle filter (Biosharp), during which the GelMA hydrogel concentration was 5%. The 10% and 15% (w/v) GelMA hydrogel were prepared by regulating the GelMA ratio. The prepared GelMA hydrogels were protected from light and stored at 4 °C. For the photo-crosslinking formation of GelMA hydrogels, each hydrogel unit needs to be irradiated by ultraviolet (UV) light (405 nm, 25 mW/cm$^2$) for 30 s at room temperature.

#### *2.1.2 Nuclear magnetic resonance (NMR)*

Gelatin and GelMA monomers were examined separately through hydrogen-1 nuclear magnetic resonance ($^1$H NMR) spectroscopy (NMR, Bruker 400 M, Fällanden, Switzerland) to detect whether methacrylate anhydride (MA) was bound to the GelMA. In brief, the gelatin and synthesized prepolymer GelMA were dissolved in deuterium oxide ($D_2O$) and detected through $^1$H NMR spectroscopy. The data was analyzed using MestReNova software.

#### *2.1.3 Scanning electron microscopy (SEM)*

Under the steps for GelMA hydrogel synthesis (discussed previously), we prepared hydrogels with different concentrations, with a diameter of 10 mm and a height of 5 mm. The surface morphology of all GelMA hydrogels was monitored by scanning electron microscopy (SEM; Zeiss Gemini 300, Oberkochen, Germany). Before the observation, the GelMA hydrogel scaffold was placed in a − 40 °C freeze-drying cabinet (SIM, Los Angeles, CA, USA). After freeze-drying, the scaffolds were fractured to obtain cross-sections and sputter-coated with gold for 30 s. The pore sizes of the GelMA hydrogel samples were measured and analyzed using ImageJ software (National Institute of Health, Bethesda, MD, USA). Briefly, we randomly selected five regions in the SEM images obtained from each group of hydrogels and analyzed the pores with uniform transverse and longitudinal diameters.

#### *2.1.4 Water retention rate*

The weight of the freeze-dried hydrogels with different hydrogel scaffold concentrations was recorded as $W_1$, while that after soaking PBS for a day at 37 °C was recorded as $W_2$. Following this, the wet hydrogel scaffold was weighed at 37 °C as $W_t$ per hour. The water retention ($W_R$) was recorded every hour as $W_R = (W_t - W_1)/W_2 \times 100\%$. Each treatment was repeated three times, and each experiment contained three samples.

#### *2.1.5 Young's modulus*

GelMA hydrogels were prepared in advance in a mold (diameter, 10 mm; height, 5 mm) and every hydrogel unit was irradiated to gelatinize under a UV light (405 nm, 25 mW/cm$^2$) for 30 s. The UV-gelatinized scaffolds were then placed in PBS, and soaked for 24 h at 37 °C for subsequent analysis. A mechanical testing instrument (E10000, Instron, Norwood, MA, USA) was used to measure Young's modulus at 2 mm/min compression speed and 1.2 mm compression distance. Each group of experiments was repeated three times.

#### 2.1.6 Water contact angle

Different concentrations of the hydrogel scaffolds were prepared in advance to evaluate their hydrophilicity by water contact angle (WCA). First, 2.5 μL of deionized water was dripped on the surface of the prepared hydrogel scaffolds during camera recording. Then, a contact angle goniometer (E10000, Instron, Norwood, MA, USA) was employed to measure the WCA of each hydrogel scaffold, using the image of the droplet shape. Each group of experiments was repeated three times.

### 2.2 Cell extraction and culture

The NPCs and AFSCs were prepared as described in our previous work [11, 41]. PBS and 5% penicillin/streptomycin (Beyotime, Shanghai, China) were added to a six-well plate. The skin and fascia of a rat tail were peeled off with a scalpel to expose the IVD, which was cut horizontally. The cut disk was placed in PBS for cleaning; the AF tissue on the outer edge and the NP tissue was removed with forceps and a scalpel. The stripped NP and AF tissues were placed in a six-well plate for rapid washing. For the extraction of NPCs, the removed NP tissue was digested in 2 mL of type-II collagenase (0.2% w/v, Yeasen, Shanghai, China) for 1 h. The added type-II collagenase should cover the NP tissue. The digested NP tissue was then washed and centrifuged. NPCs were cultured in a growth medium including DMEM/F12 (Gibco) basic medium, 10% fetal bovine serum (FBS, Gibco), and 1% penicillin /streptomycin (Invitrogen, Carlsbad, CA, USA), and then transferred to an incubator at 37 °C and 5% CO2. Conversely, AF tissue digestion required a serum-free medium containing type-I (Yeasen) and type-II collagenase. The culture was maintained in an incubator, and the culture medium was replaced regularly.

### 2.3 Fabrication of graded-3D NPC- and AFSC-seeded annular scaffolds

The integrated scaffold was designed with a concentric graded structure having four layers and a 1.5-mm thickness. The diameters of the concentric layers were 1, 2, 3, and 4 mm from the inner to outer layers, respectively. The innermost layer had $1 \times 10^5$ NPCs encapsulated in 5% photosensitive GelMA under UV light. The other three layers (inward to outward) contained AFSCs ($1 \times 10^5$, $2 \times 10^5$, and $4 \times 10^5$ cells) encapsulated in GelMA hydrogel (5%, 10%, and 15%, respectively) (Fig. 1). The prepared scaffold was placed immediately in a growth medium and then cultured in an incubator at 37 °C and 5% $CO_2$. The growth medium was changed every three days.

### 2.4 Cytocompatibility

#### 2.4.1 Live/dead assay

A total of $4 \times 10^6$ cells/mL NPCs and AFSCs were each suspended and mixed with the GelMA hydrogel at different concentrations. The suspensions were added to a mold with a diameter of 5 mm and a height of 2 mm and gelatinized under UV light. To detect the viability of the different concentrations, GelMA-encapsulated cells were cultured in a growth medium in an incubator at 37 °C and 5% $CO_2$. On days 3 and 7, the hydrogel scaffolds were stained using the live/dead stain working solution in the Live/Dead Kit (Yeasen, Shanghai, China), following the manufacturer's instructions. Briefly, we first performed a tenfold dilution of 10 × Assay Buffer, then thoroughly mixed 5 mL of the dilution with 15 μL of PI and 5 μL of Calcein-AM, and, finally, co-incubated the mixture and co-cultured the scaffold. After incubation at 37 °C for 30 min, 1 × Assay Buffer washing was performed three times, and the survival of the seeded cells was evaluated using a laser scanning confocal microscope (LSCM; Olympus, Tokyo, Japan). Subsequently, images were captured and statistical analysis was performed.

#### 2.4.2 Cell adhesion

Nuclear skeleton staining was conducted on the actin filaments to analyze the cell adhesion in the integrated scaffold. In brief, the GelMA hydrogels of different concentrations were added to a 96-well plate. NPCs and AFSCs were seeded into each well at a density of $2 \times 10^3$ cells/well. The scaffold with co-loaded cells was cultured in a growth medium. After incubation for 7 days in the medium, the cells were washed twice with PBS, fixed with 4% paraformaldehyde (Beyotime) for 30 min, and permeabilized with 0.1% Triton (Solarbio, Beijing, China) for 5 min. Staining was then performed with FITC-phalloidin (Invitrogen, Shanghai, China) in the dark at 25 °C for 20 min, followed by incubation with DAPI solution (1:200, Cyagen, Guangzhou, China) for 5 min. After washing the cells with PBS, images were obtained using fluorescence microscopy (ZEISS). The average cell area of the AFSCs and NPCs were analyzed using ImageJ software.

#### 2.4.3 Immunofluorescence analysis

Immunofluorescence staining was performed to observe the expression of Col-I, Col-II, and AGG. In short, the cell-encapsulated hydrogel scaffolds were prepared as described above and cultured in a six-well plate at 37 °C and 5% $CO_2$ for 14 days, followed by fixation, gradient dehydration, and OCT (Sakura, Chiba, Japan) embedding.

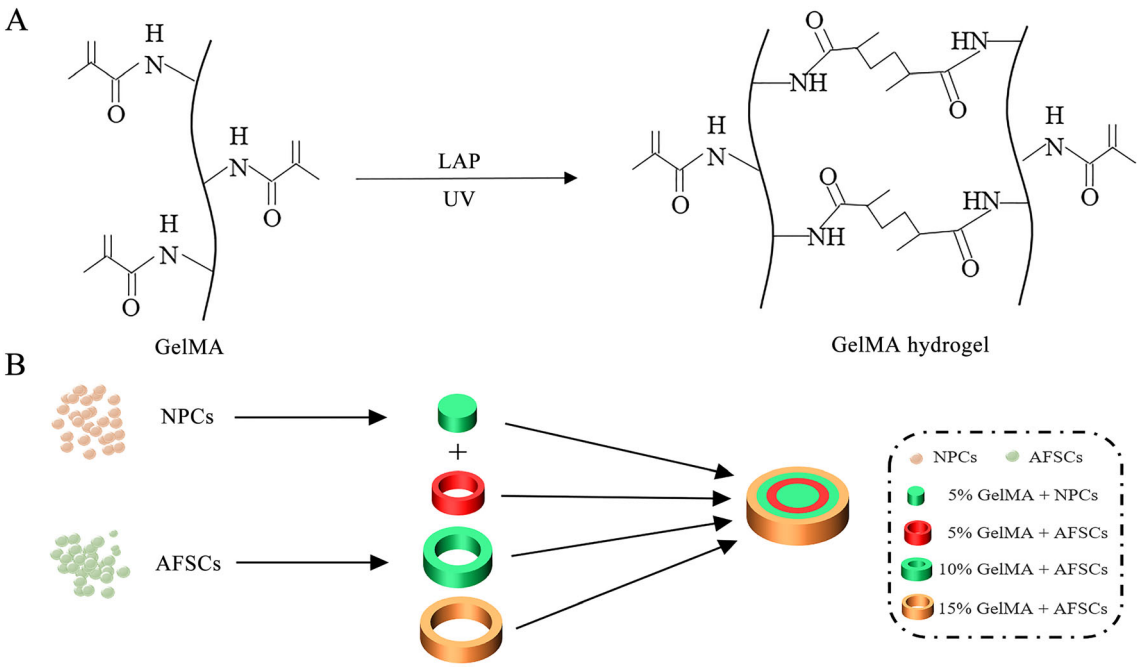


**Fig. 1** Schematic diagram of the experimental idea **A** Schematic representation of GelMA hydrogel crosslinking. **B** Schematic representation of the 3D annular scaffold integrated with graded GelMA hydrogel

Sections were obtained and subjected to antigen repair using an EDTA antigen repair solution (Servicebio, Wuhan, China). BSA (Servicebio) was used to block the sections for 2 h. Dilutions containing primary antibodies Col-I (1:200, Affinity, Jiangsu, China), Col-II (1:200, Affinity), and AGG (1:200, Affinity) polyclonal antibodies were added to the sections at 4 °C overnight, followed by dilution with goat anti-rabbit, CY3-conjugated secondary antibody (1:200, Affinity) in the dark for another 2 h. Finally, glycerol nuclear staining was performed. The sections were sealed, prepared on slides, and observed under a fluorescence microscope (ZEISS). Then, the images were captured, and statistical analysis was performed.

#### *2.4.4 Migration experiment*

The migration of cells was observed using traced cells in the graded 3D annular hydrogel. In short, the NPC and AFSC suspensions at $1 \times 10^6$ cell/mL were centrifuged and the supernatant was discarded. The remaining fraction was cultured in an incubator with a red, green, and orange tracer reagent (Proteintech, Wuhan, China) for 20 min. This procedure was repeated twice. The traced cells were harvested and mixed with hydrogels of different concentrations. The annular hydrogel scaffold was prepared as described above. The NPCs were mixed with 5% GelMA hydrogel to form the inner layer of the scaffold ($1 \times 10^5$ cells), and the AFSCs were mixed with 5%, 10%, and 15% hydrogel to form the three outer layers of the scaffold ($1 \times 10^5$, $2 \times 10^5$, and $4 \times 10^5$ cells), and the constructed integrated scaffold was cross-linked using UV light. Finally, the integrated scaffold was placed in a culture medium for 7 and 14 days and microscopically observed. The cell migration distances were analyzed using ImageJ software.

### 2.5 Statistical analysis

All the obtained data are expressed as the mean ± standard deviation and were analyzed using SPSS 20.0 and GraphPad Prism 8.0. One-way analysis of variance and two-sample independent t-tests were used for data comparison between the groups. Statistical significance was set at $p < 0.05$.

## 3 Results

### 3.1 Characterization of GelMA hydrogel scaffolds with different concentrations

In this study, GelMA was formed by the substitution reaction between the amino groups of gelatin and the methacryloyl groups of MA. Consequently, the functional groups of GelMA were cross-linked under UV irradiation in the presence of a photo-initiator. To verify the successful binding of MA to gelatin, the synthesized monomer, GelMA, and gelatin were dissolved in $D_2O$ at room

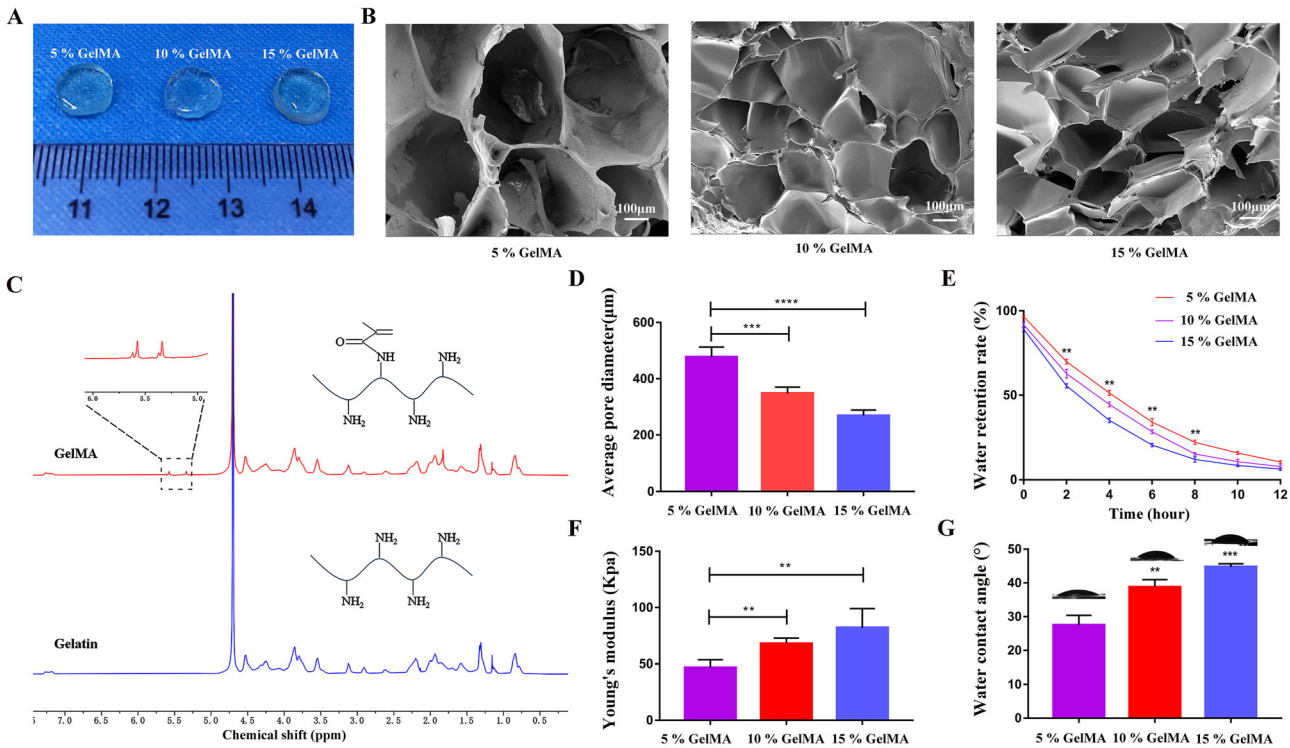


**Fig. 2** GelMA hydrogel characterization. **A** The GelMA hydrogels at different concentrations. **B** Scanning electron microscopy (SEM) images at the micron scale of GelMA hydrogels at different concentrations (scale bar: 100 μm). **C** Hydrogen-1 nuclear magnetic resonance ($^1$H NMR) spectra of gelatin and GelMA hydrogels prepared in deuterium oxide ($D_2O$) at room temperature. **D** Average pores of GelMA hydrogels at different concentrations. **E** Water retention property of GelMA hydrogels. **F** Average compression modulus of GelMA hydrogels. **G** Water contact angle (WCA) of GelMA hydrogels. (*$p < 0.05$, **$p < 0.01$, ***$p < 0.001$)

temperature and detected through $^1$H NMR spectroscopy. As shown in Fig. 2, the characteristic alkene hydrogen peak of acrylamide in the GelMA appeared at 5.33 and 5.57 ppm; which is congruent with previously established research [42].

The hydrogel scaffolds with different concentrations were fabricated by regulating the GelMA ratio. As shown in the SEM images in Fig. 2B, the hydrogels with different concentrations all displayed a honeycomb-like porous structure, which promoted the transport of nutrients and provided sufficient space for cell proliferation and adhesion. The average pore size of the 5%, 10%, and 15% hydrogels was 434.2 μm, 329.4 μm, and 245.9 μm (Fig. 2D), respectively, indicating that the pore size gradually decreased with increasing hydrogel concentration.

The water retention rate is another important characteristic of the hydrogel water content. Over time, we found a decreasing trend in the water retention rate of hydrogels with different concentrations (Fig. 2E). However, the rate of the 5% hydrogel was always higher than that of the other two groups; at 12 h the water retention of the 5%, 10%, and 15% hydrogels was 10.33%, 7.67%, 6.23%, respectively.

Hydrogel elasticity also has a critical impact on cell adhesion. To investigate the relationship between the mechanical strength and hydrogel concentration, compression tests were conducted using 5%, 10%, and 15% (w/v) GelMA hydrogels. Results demonstrated that the 5% hydrogel had the lowest compression modulus compared with the other two groups, and a positive relationship was identified between the hydrogel concentration and Young's modulus (Fig. 2F).

Hydrogel elasticity plays an essential role in water contact angle in determining hydrophilicity, and high water content is more likely to promote cell survival. In our experiments, the water contact angles of the 5%, 10%, and 15% hydrogels were 27.5° ± 1.4°, 38.75° ± 1.1°, 44.75° ± 0.48° (Fig. 2G), respectively, which may be related to the level of cross-linking of the hydrogel. The experiments revealed that the 5% hydrogel had a higher water content and, therefore, was more favorable for cell survival.

### 3.2 Cell survival in the differently concentrated hydrogel scaffolds

To investigate the viability of cells encapsulated in different concentrations of hydrogels, live/dead staining was performed to determine cell survival in the integrated

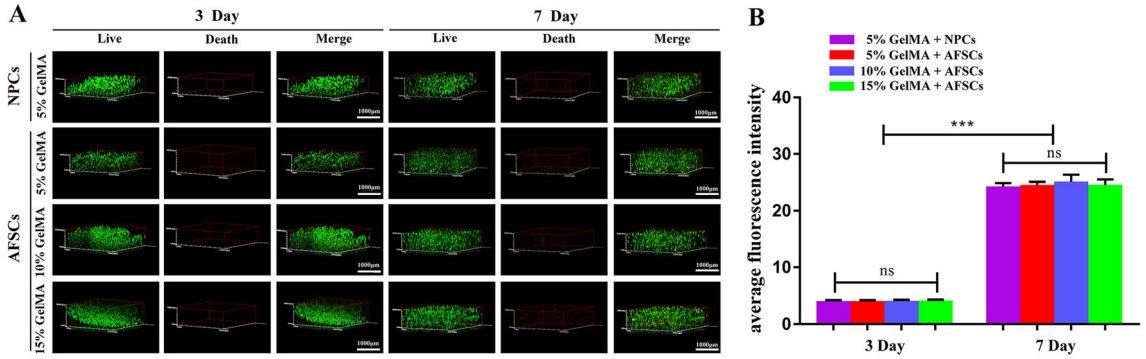


**Fig. 3** Laser scanning confocal images of the integrated GelMA hydrogel scaffold at different concentrations, encapsulating NPCs and AFSCs. **A** Green fluorescence (Calcein-AM) represents the living cells, and red fluorescence (PI) represents the dead cells (scale bar: 1000 μm). **B** Quantitative analysis for the mean PI fluorescence intensity in GelMA hydrogel of different concentrations (*$p < 0.05$, **$p < 0.01$, "ns" for "not significant")

scaffold on day 3 and day 7 (Fig. 3). The immunofluorescence results demonstrated that the majority of cells encapsulated in different concentrations of hydrogels remained viable on day 3, and hardly any dead cells were detected. By the time the incubation reached day 7, there was an increase in dead cells in each hydrogel scaffold compared to day 3, with no significant difference in the number of dead cells between the scaffolds. Interestingly, the cells encapsulated in the hydrogels still maintained a high activity on day 7. The results showed that the cells encapsulated in different concentrations of hydrogel presented a high activity on days 3 and 7, indicating that all the hydrogel scaffolds exhibited good biocompatibility and non-toxicity.

### 3.3 Cell adhesion in the differently concentrated hydrogel scaffolds

The adhesion of the different scaffolds has an important effect on cell morphology. Our experiments demonstrated that the morphology of actin filaments for AFSCs and NPCs on the surface of 5% hydrogels was ample and displayed good ductility (Fig. 4A). Cells were able to adhere and spread efficiently on the surface of 5% hydrogels. In contrast, the morphology of the attached cells tended to be round when AFSCs adhered to the surface of 10% and 15% hydrogels, and this situation became more evident with increasing hydrogel concentrations. The average cell area, which was measured and calculated using Image J software, of the AFSCs and NPCs on the surface of 5% hydrogels was significantly higher than that on the 10% and 15% hydrogels (Fig. 4B). These differences indicate

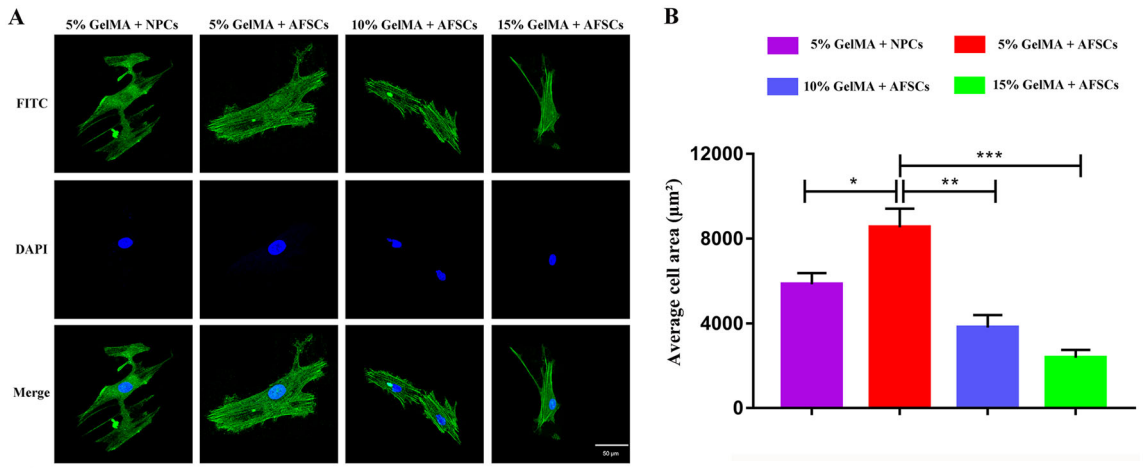


**Fig. 4** Adhesion of nucleus pulposus cells (NPCs) and annulus fibrosus-derived stem cells (AFSCs) on the GelMA hydrogel surface. **A** FITC-labeled phalloidin/DAPI staining of actin filaments and nuclei in NPCs and AFSCs on different concentrations of GelMA hydrogels after 7 days. **B** Quantitative analysis for the average cell area of NPCs and AFSCs on the GelMA hydrogel surface (*$p < 0.05$, **$p < 0.01$, ***$p < 0.001$, relative to the control group)

that 5% hydrogels provide an adhesive surface that enhances cell–hydrogel interactions compared to 10% and 15% hydrogels, and that the adhesive nature of the high-concentration hydrogel scaffold limits cell growth; this may be related to the pore size, with larger pores being more conducive to cell stretching.

### 3.4 Immunofluorescence analysis

The expression of proteins for NPCs and AFSCs encapsulated in different concentrations of hydrogels was evaluated by immunofluorescence. As shown in Fig. 5, the expression of Col-I was significantly lower in AFSCs encapsulated in 10% and 15% GelMA hydrogels compared to the 5% hydrogels. This indicates that as the hydrogel concentration increases, AFSCs have less effect on the expression of Col-I, which may be influenced by the photo-crosslinking density of the hydrogel. This phenomenon also coincides with the verification of the adhesion properties for cells in differently concentrated hydrogel scaffolds. For NPCs encapsulated in 5% hydrogels, a slight expression of Col-I was observed. Col II and AGG are crucial components of the NP tissue. Based on the optical density measurements, the expression of AGG and Col II in NPCs in 5% hydrogel was significantly higher than that of AFSCs in the three differently concentrated hydrogels. However, there was no significant difference in the expression of AGG and Col II among the three AFSC hydrogels (Fig. 5B). Collectively, Col-II and AGG were more highly expressed in the NP to the AF, which is consistent with the natural protein expression pattern in the IVD.

### 3.5 Hydrogel-encapsulated cell migration in the 3D annular scaffold

The 3D integrated scaffold is composed of a four-layer concentric structure where AFSCs and NPCs are encapsulated in differently concentrated hydrogel scaffolds. Figure 6 presents the immunofluorescence image of the encapsulated fluorescent probe cells in a section on day 1. In the different levels, cells are labeled with different colored fluorescent probes. The innermost layer is 5% GelMA hydrogel encapsulating green probe-labeled NPCs. From the inside to the outside, the layers contained 5%, 10%, and 15% GelMA hydrogel, encapsulating AFSCs labeled with red (middle), green (outer), and orange (outermost) probes. Our success in establishing a graded 3D annular scaffold is shown by the integration of fluorescently labeled cells with hydrogel scaffolds. We also examined the migration of cells in the bionic scaffold between the different levels on days 7 and 14. As shown in Fig. 6B, I/II, II/III, and III/IV refer to the 2D/3D immunofluorescence image of the junction between the layers. On day 7, the number of cells inter-migrating between the layers was low, but the inter-penetration and migration of cells between the layers could be seen on day 14. Then, by measuring the cell migration distances of the AFSCs and NPCs between the different layers of the scaffold using Image J software, we found a significant difference in the cell spreading distances on day 14 in all the layers compared to that on day 7. At the interface between the 5% and 10% hydrogels, it was observed that the cells have further spreading distances than those at the interface of the 15% hydrogels on day 14, which may be caused by the high mechanical properties of the hydrogels limiting cell spreading, resulting in less efficient cell

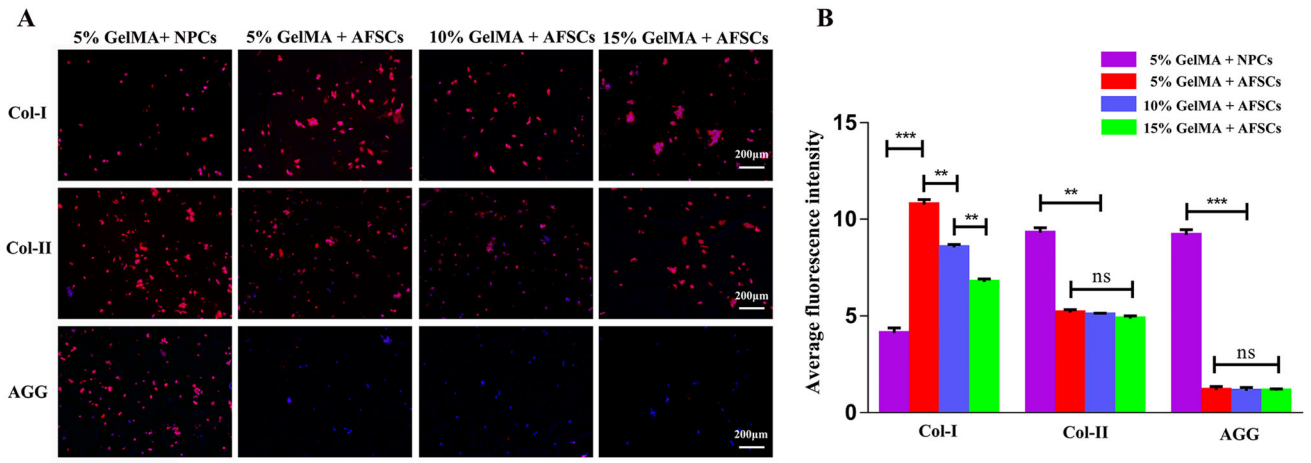


**Fig. 5** Expression of Col-I, Col-II, and AGG for NPCs and AFSCs encapsulated in GelMA hydrogel of different concentrations. **A** Immunofluorescence expression of Col-I, Col-II, and AGG for NPCs and AFSCs on day 14 (scale bar: 200 μm). **B** Quantitative analysis for the average fluorescence intensity between different groups (*$p < 0.05$, **$p < 0.01$, ***$p < 0.001$, relative to the control group)

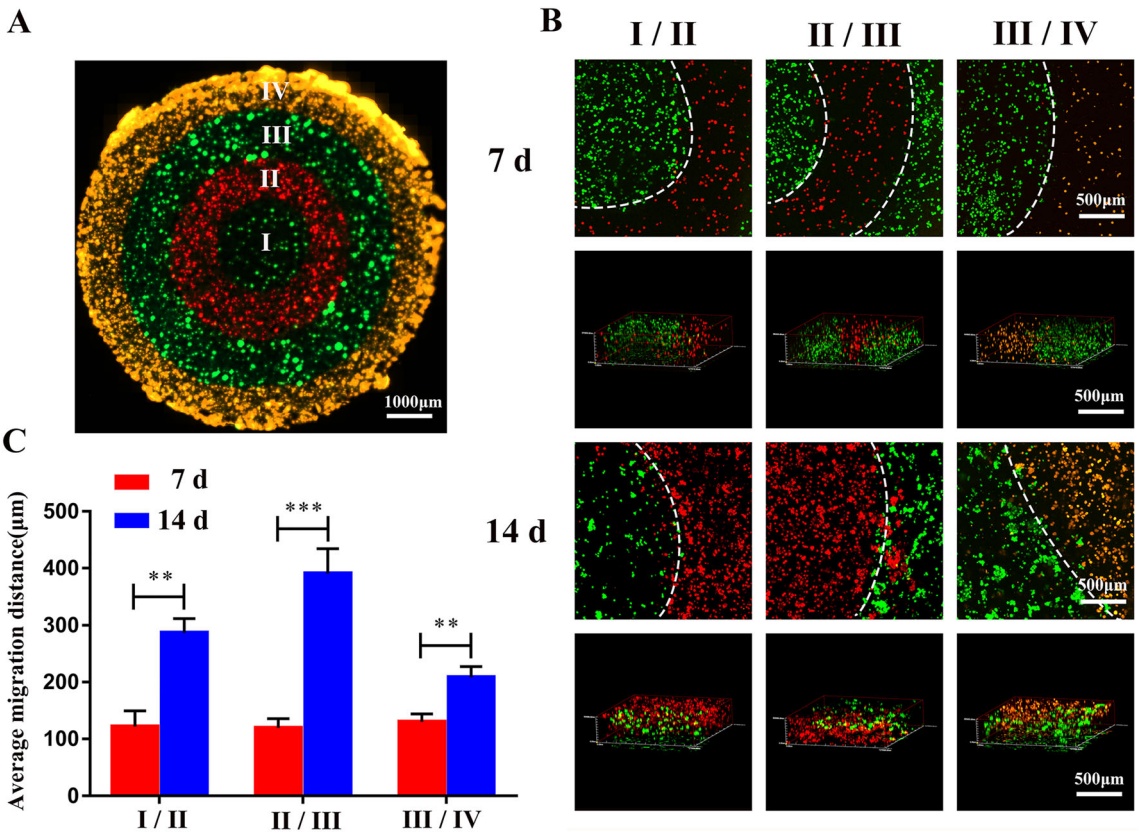


**Fig. 6** Cell tracing in the integrated scaffold. **A** Immunofluorescence image of frozen cell sections of the annular scaffold on day 1 (scale bar: 1000 μm). **B** 2D/3D Immunofluorescence images of cell migration in four different hydrogel layers on days 7 and 14 (scale bar: 500 μm). The dotted line represents the dividing line between the different hydrogel layers. **C** Quantitative analysis for the average cell migration distance in four different hydrogel layers between days 7 and 14. (*$p < 0.05$, **$p < 0.01$, ***$p < 0.001$, relative to the control group)

migration. This also demonstrates that the bionic scaffold has good biocompatibility and that the integrated scaffolds acting as a cell carriers can promote cell survival, migration, and protein expression.

## 4 Discussion

Tissue-engineered regenerative materials for treating IVD degeneration have been gaining attention for their well-suited bioactivity and biocompatibility. The biological repair strategy based on cell transplantation and scaffolds has a significant effect on treating disc herniation. In the present study, an annular integrated scaffold with gradient concentrations of GelMA, integrated with NPCs and AFSCs, was constructed. By adjusting the concentration of the hydrogel, this cell-loaded photo-crosslinked GelMA hydrogel shows unique biological properties, including cell survival, cell extension, and protein expression. The experiments demonstrated that hydrogels with different mechanical properties were beneficial for cell survival. Additionally, the corresponding extracellular matrix (ECM) components are secreted to allow for the simulation of the natural IVD. The construction of cell-loaded integrated scaffolds will be an effective strategy for treating disc degeneration.

The NP, surrounded by the AF, produces ECM components, mainly proteoglycans and type II collagen [43, 44]. A healthy nucleus pulposus tissue needs to be soft and flexible to cope with higher buffering stresses. The characteristic changes occurring in the NP tissue with age include apoptosis, and reduction of collagen and other content, which leads to water loss [45]. These changes may render the outer AF mechanically impaired, enabling the NP tissue to protrude, resulting in nerve compression and clinical symptoms (disc herniation) [46]. Therefore, water retention and certain mechanical properties of the scaffold are important for maintaining mechanical stability and survival of co-loaded cells. The measurements of both the compressive modulus and water contact angle of hydrogels with different concentrations revealed good mechanical and hydration properties, which play a vital role in simulating the physiological structure of IVDs. GelMA hydrogel is a popular tissue-engineering material owing to its

various advantages, including 3D form, large aspect ratio, dense fiber network, and strong biocompatibility [47], which support the multi-differentiation of seeded cells into bone, nerve, vascular, and IVD tissues. Compared to conventional scaffolds, we can modulate the physical properties of the scaffolds by changing the GelMA ratio or crosslinking times [28]. The physical properties include compression modulus [48, 49], porosity, and degradation properties [50]. The different physical properties and cellular response parameters of GelMA hydrogels allow their use in different biomedical applications. In natural IVD, the histologic characteristic of insufficient blood supply makes cell-seeded grafting a better therapy, but the bioactivity of the seed cells can be affected by the physicochemical gradient of tissue-engineered materials [51–53]. Modulating the physical properties of GelMA hydrogels by controlling the synthesis process has different implications for the proliferation, survival, differentiation, and extension of different cells. Related experimental studies have shown that the proliferation and differentiation of neural stem cells co-cultured with bone mesenchymal stem cells (BMSCs) can be influenced by modulating the mechanical properties of the hydrogels [11]. In our experimental study, hydrogels with different mechanical strengths were tested *in vitro* for cell viability to facilitate cell survival. The presence in gelatin of an arginine-glycine-aspartate adhesion domain and matrix metalloproteinase (MMP)-sensitive sites allows the combination with different types of growth factors to promote the proliferation and survival of different types of cells within the scaffold [54]. Nevertheless, hydrogels with different physical properties all have a loose and porous structure, which is more conducive to the exchange and transport of nutrients. However, with the increase of mechanical strength, the porosity of the hydrogel becomes smaller; the low concentration hydrogel is affected by the large grid size of the low cross-link density, thus the pores are larger. More importantly, for high concentration hydrogels, the high crosslink density limits the expansion of cells (Fig. 4), which is well verified in the present experimental study [11], where cells wrapped in high concentration hydrogels exhibit poor ductility.

Cells for culture in three-dimensional (3D) microenvironments compensate for the limitations of current two-dimensional cell culture practices. The morphology and biological properties of cells in different growth microenvironments vary significantly [55], and 3D cell cultures can better reflect the biochemical and physical properties of the cellular microenvironment [56]. It is critical for the ability of cells to grow and migrate in 3D microenvironments for applications in IVD tissue regeneration engineering. Compared to conventional hydrogels, the ability of GelMA hydrogels to enhance cell binding is because of the distribution of binding sites in all the hydrogel chains [11]. The adhesion of cells to the hydrogel is promoted by the binding sites, and the loose and porous structure promotes cell growth and ECM secretion. However, hydrogels with different crosslinking densities have a great influence on the spatial distribution of ECM components. The immunofluorescence results showed the differential expression of Col-I, Col-II, and GAG in different concentrations of hydrogels (Fig. 5). This may be related to the cell type and the physical properties of the hydrogels. In the case of hydrogels, 5% GelMA hydrogels with a low crosslink density and larger pore size are more conducive to cell spreading, thus facilitating the deposition of Col-I, Col-II, and GAG. This further supports the practicability of the integrated scaffold. The cells encapsulated in the 3D GelMA scaffolds showed good migration ability, but we need to further study the molecular mechanisms and signal transduction pathways underlying the cell-specific differentiation. *In vitro* experiments identified the positive biological properties of the integrated scaffold, allowing a simulation of the natural tissues with acceptable physicochemical and biological properties. The combination of seeded cells and biodegradable GelMA hydrogel scaffolds could provide a superior platform for disc degeneration repair, in which the hydrogel scaffold acts as a carrier for cell transplantation. Tissue engineering techniques can provide better treatment options for the serious side effects and poor clinical outcomes associated with conventional surgery for disc degeneration [57]. The arginine-glycyl-aspartate adhesion sites in the GelMA hydrogel readily bind to a variety of cell types to promote cell growth and adhesion and the physiological characteristics of the GelMA hydrogel closely resemble that of the cellular microenvironment. Therefore, their use could be beneficial in tissue engineering techniques. The photo-induced crosslinking properties of the GelMA hydrogel offer many advantages over other scaffolds, such as injectability, faster gelation, bioprinting, and improved mechanical properties [58]. In particular, the injectable properties of the GelMA hydrogel allow for the combination of seed cells and precise injection into the degenerating disc [59], which reduces tissue damage and allows for precise treatment compared to traditional open surgery. Therefore, the bionic scaffold that was built in this study by constructing a GelMA hydrogel carrying seeded cells, utilized the advantageous physical properties of the GelMA hydrogel and provided a promising design for clinical precision treatment of disc degeneration, which has certain guiding significance. Although the cell-encapsulated integration scaffold was not validated with *in vivo* experiments, our study provides a theoretical basis for simulating the microstructure of natural IVD tissues *in vivo* and provides a new approach for treating IVD degeneration.

**Acknowledgements** This study was supported by grants from the Natural Science Foundation of Anhui Province (2008085QH362), 512 Talents Development Project of Bengbu Medical College (by51202302), and the Scientific Research Foundation of Bengbu Medical College (BYKY1884, BYKY2019039ZD, 2020byzd070 and 2021bypd006).

**Author Contribution** YM (Doctor of Philosophy), TQ (Doctor of Medicine), and ZL (Master of Medicine) were involved in study design, literature research, data analysis, and writing the manuscript. YZ (Master of Medicine), YZ (Master of Medicine), ZL (Master of Medicine), ZZ (Master of Medicine) and XG (Master of Medicine) were involved in the study design and data analysis.

**Declarations**

**Conflict of interest** The authors have no financial conflicts of interest.

**Ethical statement** This study was approved by the ethics committee of the medical faculty of Bengbu Medical College (Approval Number No. 2019100).

## References

1. Risbud MV, Shapiro IM. Role of cytokines in intervertebral disc degeneration: pain and disc content. Nat Rev Rheumatol. 2014;10:44–56.
2. Dowdell J, Erwin M, Choma T, Vaccaro A, Iatridis J, Cho SK. Intervertebral disk degeneration and repair. Neurosurgery. 2017;80:S46–54.
3. Yang S, Zhang F, Ma J, Ding W. Intervertebral disc ageing and degeneration: the antiapoptotic effect of oestrogen. Ageing Res Rev. 2020;57:100978.
4. Hudson KD, Alimi M, Grunert P, Härtl R, Bonassar LJ. Recent advances in biological therapies for disc degeneration: tissue engineering of the annulus fibrosus, nucleus pulposus and whole intervertebral discs. Curr Opin Biotechnol. 2013;24:872–9.
5. Lazebnik M, Singh M, Glatt P, Friis LA, Berkland CJ, Detamore MS. Biomimetic method for combining the nucleus pulposus and annulus fibrosus for intervertebral disc tissue engineering. J Tissue Eng Regen Med. 2011;5:e179–87.
6. Bruehlmann SB, Rattner JB, Matyas JR, Duncan NA. Regional variations in the cellular matrix of the annulus fibrosus of the intervertebral disc. J Anat. 2002;201:159–71.
7. Zhu L, Yu C, Zhang X, Yu Z, Zhan F, Yu X, et al. The treatment of intervertebral disc degeneration using traditional Chinese medicine. J Ethnopharmacol. 2020;263:113117.
8. Cazzanelli P, Wuertz-Kozak K. MicroRNAs in Intervertebral disc degeneration, apoptosis, inflammation, and mechanobiology. Int J Mol Sci. 2020;21:3601.
9. Chan WC, Sze KL, Samartzis D, Leung VY, Chan D. Structure and biology of the intervertebral disk in health and disease. Orthop Clin North Am. 2011;42:447–64.
10. Huang B, Zhuang Y, Li CQ, Liu LT, Zhou Y. Regeneration of the intervertebral disc with nucleus pulposus cell-seeded collagen II/hyaluronan/chondroitin-6-sulfate tri-copolymer constructs in a rabbit disc degeneration model. Spine (Phila Pa 1976). 2011;36:2252–59.
11. Xu P, Guan J, Chen Y, Xiao H, Yang T, Sun H, et al. Stiffness of photocrosslinkable gelatin hydrogel influences nucleus pulposus cell properties in vitro. J Cell Mol Med. 2021;25:880–91.
12. Horner HA, Urban JP. 2001 Volvo award winner in basic science studies: effect of nutrient supply on the viability of cells from the nucleus pulposus of the intervertebral disc. Spine (Phila Pa 1976). 2001;26:2543–9.
13. Ma CJ, Liu X, Che L, Liu ZH, Samartzis D, Wang HQ. Stem cell therapies for intervertebral disc degeneration: immune privilege reinforcement by Fas/FasL regulating machinery. Curr Stem Cell Res Ther. 2015;10:285–95.
14. Mohammadian M, Abasi E, Akbarzadeh A. Mesenchymal stem cell-based gene therapy: a promising therapeutic strategy. Artif Cells Nanomed Biotechnol. 2016;44:1206–11.
15. Kang HW, Lee SJ, Ko IK, Kengla C, Yoo JJ, Atala A. A 3D bioprinting system to produce human-scale tissue constructs with structural integrity. Nat Biotechnol. 2016;34:312–9.
16. Sharma P, Kumar P, Sharma R, Bhatt VD, Dhot PS. Tissue engineering; current status and futuristic scope. J Med Life. 2019;12:225–9.
17. Sharma R, Kumar S, Bhawna, Gupta A, Dheer N, Jain P, et al. An insight of nanomaterials in tissue engineering from fabrication to applications. Tissue Eng Regen Med. 2022. https://doi.org/10.1007/s13770-022-00459-z
18. Silva-Correia J, Gloria A, Oliveira MB, Mano JF, Oliveira JM, Ambrosio L, et al. Rheological and mechanical properties of acellular and cell-laden methacrylated gellan gum hydrogels. J Biomed Mater Res A. 2013;101:3438–46.
19. Sun Z, Luo B, Liu Z, Huang L, Liu B, Ma T, et al. Effect of perfluorotributylamine-enriched alginate on nucleus pulposus cell: Implications for intervertebral disc regeneration. Biomaterials. 2016;82:34–47.
20. Roughley P, Hoemann C, DesRosiers E, Mwale F, Antoniou J, Alini M. The potential of chitosan-based gels containing intervertebral disc cells for nucleus pulposus supplementation. Biomaterials. 2006;27:388–96.
21. Collin EC, Grad S, Zeugolis DI, Vinatier CS, Clouet JR, Guicheux JJ, et al. An injectable vehicle for nucleus pulposus cell-based therapy. Biomaterials. 2011;32:2862–70.
22. Cruz MA, Hom WW, DiStefano TJ, Merrill R, Torre OM, Lin HA, et al. Cell-seeded adhesive biomaterial for repair of annulus fibrosus defects in intervertebral discs. Tissue Eng Part A. 2018;24:187–98.
23. Li X, Fan C, Xiao Z, Zhao Y, Zhang H, Sun J, et al. A collagen microchannel scaffold carrying paclitaxel-liposomes induces neuronal differentiation of neural stem cells through Wnt/beta-catenin signaling for spinal cord injury repair. Biomaterials. 2018;183:114–27.
24. Chen Z, Wu H, Wang H, Zaldivar-Silva D, Aguero L, Liu Y, et al. An injectable anti-microbial and adhesive hydrogel for the effective noncompressible visceral hemostasis and wound repair. Mater Sci Eng C Mater Biol Appl. 2021;129:112422.
25. Yu Y, Wang Y, Zhang W, Wang H, Li J, Pan L, et al. Biomimetic periosteum-bone substitute composed of preosteoblast-derived matrix and hydrogel for large segmental bone defect repair. Acta Biomater. 2020;113:317–27.
26. Zhao X, Li S, Du X, Li W, Wang Q, He D, et al. Natural polymer-derived photocurable bioadhesive hydrogels for sutureless keratoplasty. Bioact Mater. 2022;8:196–209.
27. Yan Y, Cao Y, Cheng R, Shen Z, Zhao Y, Zhang Y, et al. Preparation and in vitro characterization of gelatin methacrylate for corneal tissue engineering. Tissue Eng Regen Med. 2022;19:59–72.
28. Chen YC, Lin RZ, Qi H, Yang Y, Bae H, Melero-Martin JM, et al. Functional human vascular network generated in photocrosslinkable gelatin methacrylate hydrogels. Adv Funct Mater. 2012;22:2027–39.
29. Zhou P, Xu P, Guan J, Zhang C, Chang J, Yang F, et al. Promoting 3D neuronal differentiation in hydrogel for spinal cord regeneration. Colloids Surf B Biointerfaces. 2020;194:111214.

30. Zhou J, Tian Z, Tian Q, Peng L, Li Q, Luo X, et al. 3D bioprinting of a biomimetic meniscal scaffold for application in tissue engineering. Bioact Mater. 2021;6:1711–26.
31. Qiao Z, Lian M, Han Y, Sun B, Zhang X, Jiang W, et al. Bioinspired stratified electrowritten fiber-reinforced hydrogel constructs with layer-specific induction capacity for functional osteochondral regeneration. Biomaterials. 2021;266:120385.
32. Hu H, Dong L, Bu Z, Shen Y, Luo J, Zhang H, et al. miR-23a-3p-abundant small extracellular vesicles released from Gelma/nanoclay hydrogel for cartilage regeneration. J Extracell Vesicles. 2020;9:1778883.
33. Sultan MT, Choi BY, Ajiteru O, Hong DK, Lee SM, Kim HJ, et al. Reinforced-hydrogel encapsulated hMSCs towards brain injury treatment by trans-septal approach. Biomaterials. 2021;266:120413.
34. Ratheesh G, Vaquette C, Xiao Y. Patient-specific bone particles bioprinting for bone tissue engineering. Adv Healthc Mater. 2020. https://doi.org/10.1002/adhm.202001323
35. Qiao Y, Liu X, Zhou X, Zhang H, Zhang W, Xiao W, et al. Gelatin templated polypeptide co-cross-linked hydrogel for bone regeneration. Adv Healthc Mater. 2020;9:e1901239.
36. Monteiro MV, Gaspar VM, Ferreira LP, Mano JF. Hydrogel 3D in vitro tumor models for screening cell aggregation mediated drug response. Biomater Sci. 2020;8:1855–64.
37. Yue X, Nguyen TD, Zellmer V, Zhang S, Zorlutuna P. Stromal cell-laden 3D hydrogel microwell arrays as tumor microenvironment model for studying stiffness dependent stromal cell-cancer interactions. Biomaterials. 2018;170:37–48.
38. Eke G, Mangir N, Hasirci N, MacNeil S, Hasirci V. Development of a UV crosslinked biodegradable hydrogel containing adipose derived stem cells to promote vascularization for skin wounds and tissue engineering. Biomaterials. 2017;129:188–98.
39. Liu T, Weng W, Zhang Y, Sun X, Yang H. Applications of gelatin methacryloyl (GelMA) hydrogels in microfluidic technique-assisted tissue engineering. Molecules. 2020;25:5305.
40. Fan L, Liu C, Chen X, Zou Y, Zhou Z, Lin C, et al. Directing induced pluripotent stem cell derived neural stem cell fate with a three-dimensional biomimetic hydrogel for spinal cord injury repair. ACS Appl Mater Interfaces. 2018;10:17742–55.
41. Chu G, Yuan Z, Zhu C, Zhou P, Wang H, Zhang W, et al. Substrate stiffness- and topography-dependent differentiation of annulus fibrosus-derived stem cells is regulated by Yes-associated protein. Acta Biomater. 2019;92:254–64.
42. Li Y, Liu C, Liu W, Cheng X, Zhang A, Zhang S, et al. Apatite formation induced by chitosan/gelatin hydrogel coating anchored on poly(aryl ether nitrile ketone) substrates to promote osteoblastic differentiation. Macromol Biosci. 2021;21:e2100262.
43. Nguyen AM, Johannessen W, Yoder JH, Wheaton AJ, Vresilovic EJ, Borthakur A, et al. Noninvasive quantification of human nucleus pulposus pressure with use of T1rho-weighted magnetic resonance imaging. J Bone Joint Surg Am. 2008;90:796–802.
44. Beckstein JC, Sen S, Schaer TP, Vresilovic EJ, Elliott DM. Comparison of animal discs used in disc research to human lumbar disc: axial compression mechanics and glycosaminoglycan content. Spine (Phila Pa 1976). 2008;33:E166–73.
45. Antoniou J, Steffen T, Nelson F, Winterbottom N, Hollander AP, Poole RA, et al. The human lumbar intervertebral disc: evidence for changes in the biosynthesis and denaturation of the extracellular matrix with growth, maturation, ageing, and degeneration. J Clin Invest. 1996;98:996–1003.
46. O'Connell GD, Leach JK, Klineberg EO. Tissue engineering a biological repair strategy for lumbar disc herniation. Biores Open Access. 2015;4:431–45.
47. Rizwan M, Chan SW, Comeau PA, Willett TL, Yim EKF. Effect of sterilization treatment on mechanical properties, biodegradation, bioactivity and printability of GelMA hydrogels. Biomed Mater. 2020;15:065017.
48. Suo H, Zhang D, Yin J, Qian J, Wu ZL, Fu J. Interpenetrating polymer network hydrogels composed of chitosan and photocrosslinkable gelatin with enhanced mechanical properties for tissue engineering. Mater Sci Eng C Mater Biol Appl. 2018;92:612–20.
49. Wang Z, Tian Z, Menard F, Kim K. Comparative study of gelatin methacrylate hydrogels from different sources for biofabrication applications. Biofabrication. 2017;9:044101.
50. Cao D, Zhang Y, Cui Z, Du Y, Shi Z. New strategy for design and fabrication of polymer hydrogel with tunable porosity as artificial corneal skirt. Mater Sci Eng C Mater Biol Appl. 2017;70:665–72.
51. Wu P, Wang L, Li W, Zhang Y, Wu Y, Zhi D, et al. Construction of vascular graft with circumferentially oriented microchannels for improving artery regeneration. Biomaterials. 2020;242:119922.
52. Yang J, Yang X, Wang L, Zhang W, Yu W, Wang N, et al. Biomimetic nanofibers can construct effective tissue-engineered intervertebral discs for therapeutic implantation. Nanoscale. 2017;9:13095–103.
53. Roseti L, Parisi V, Petretta M, Cavallo C, Desando G, Bartolotti I, et al. Scaffolds for bone tissue engineering: state of the art and new perspectives. Mater Sci Eng C Mater Biol Appl. 2017;78:1246–62.
54. Raeber GP, Lutolf MP, Hubbell JA. Molecularly engineered PEG hydrogels: a novel model system for proteolytically mediated cell migration. Biophys J. 2005;89:1374–88.
55. Modulevsky DJ, Lefebvre C, Haase K, Al-Rekabi Z, Pelling AE. Apple derived cellulose scaffolds for 3D mammalian cell culture. PLoS One. 2014;9:e97835.
56. Owen SC, Shoichet MS. Design of three-dimensional biomimetic scaffolds. J Biomed Mater Res A. 2010;94:1321–31.
57. Willems P. Decision making in surgical treatment of chronic low back pain: the performance of prognostic tests to select patients for lumbar spinal fusion. Acta Orthop Suppl. 2013;84:1–35.
58. Kurian AG, Singh RK, Patel KD, Lee JH, Kim HW. Multifunctional GelMA platforms with nanomaterials for advanced tissue therapeutics. Bioact Mater. 2022;8:267–95.
59. Xu H, Sun M, Wang C, Xia K, Xiao S, Wang Y, et al. GDF5-GelMA injectable microspheres laden with adipose-derived stem cells for disc degeneration repair. Biofabrication. 2021;13:015010.